Absence of the 90 K structural transition in CuV_2S_4 crystals grown by chemical vapour transport using $TeCl_4$

2005 J. Phys.: Condens. Matter 17 4813

(http://iopscience.iop.org/0953-8984/17/30/007)

INSTITUTE OF PHYSICS PUBLISHING JOURNAL OF PHYSICS: CONDENSED MATTER

J. Phys.: Condens. Matter **17** (2005) 4813–4823 doi:10.1088/0953-8984/17/30/007

Absence of the 90 K structural transition in CuV_2S_4 crystals grown by chemical vapour transport using $TeCl_4$

D A Crandles[1], M Reedyk[1], G Wardlaw[1], F S Razavi[1], T Hagino[2], S Nagata[2], I Shimono[3] and R K Kremer[4]

[1] Department of Physics, Brock University, St Catharines, ON, L2S 3A1, Canada
[2] Department of Materials Science and Engineering, Muroran Institute of Technology, 27-1 Mizumoto-cho, Muroran, Hokkaido 050-8535, Japan
[3] Hokkaido Industrial Technology Centre, 379 Kikyo-cho, Hakodate, Hokkaido 041-0801, Japan
[4] Max-Planck-Institut fur Festkörperforschung, Heisenbergstrasse 1, D-70569 Stuttgart, Germany

Received 6 August 2004, in final form 23 June 2005
Published 15 July 2005
Online at stacks.iop.org/JPhysCM/17/4813

Abstract

Various physical properties (magnetization, specific heat, optical reflectance, electrical resistivity) of CuV_2S_4 crystals grown by chemical vapour transport using $TeCl_4$ as the transporting agent have been measured. The data show slight differences compared to samples grown using different techniques. These differences include the absence of a sharp drop in magnetization and the absence of a peak in the heat capacity near 90 K. These differences suggest that the cubic–tetragonal phase transition near 90 K does not occur in these particular crystals. The reflectance of the same crystals has been studied from (70–20 000 cm^{-1}) for temperatures between 40 and 300 K and the data are consistent with those for a disordered metal. A high frequency absorption, perhaps an interband transition, has been observed in addition to absorption due to strongly scattered free carriers.

1. Introduction

The ternary sulfospinels exhibit many interesting physical properties including superconductivity [1] as well as temperature and pressure induced metal–insulator transitions [2]. This paper focuses on one of these compounds, CuV_2S_4, which is believed to exhibit a charge density wave (CDW) at low temperature [3, 4]. The observation of CDW in only a very few three-dimensional materials makes CuV_2S_4 notable.

The behaviour of CuV_2S_4 at low temperatures is complicated by several phase transitions. An incommensurate CDW with wavevector $\vec{q} = (\frac{1}{4} - \delta)[110]$ forms at 90 K. The incommensurability, δ, decreases until 75 K is reached where lock-in occurs and $\delta = 0$. At around 50 K a new incommensurate CDW forms with $\vec{q} \approx \frac{1}{3}[110]$ [3]. In addition to

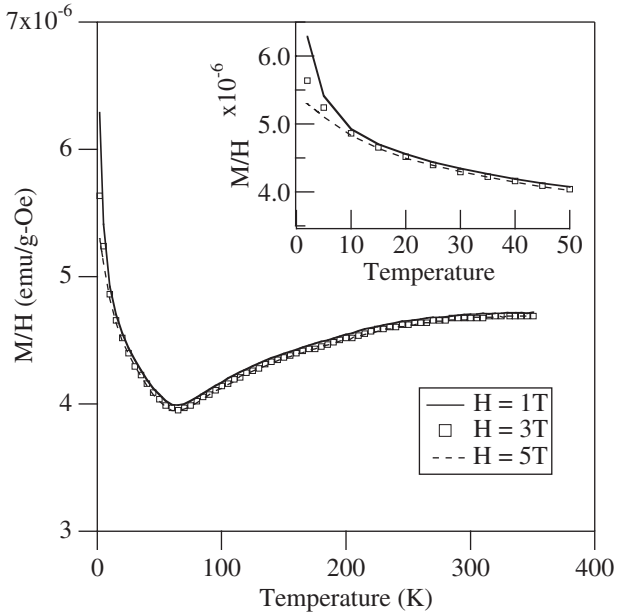

Figure 1. Ratio of magnetization (M) to magnetic field (H) as a function of temperature for three different applied fields. The samples were field cooled to 2 K, and the magnetic moment measured as the temperature was increased. Inset: expansion of the low temperature region of the main figure.

these CDW transitions, a cubic–tetragonal structural phase transition is believed to occur near 90 K [5, 6]. To complicate matters further, there is controversy regarding the low temperature symmetry of the material. It has been observed to be cubic [3] or orthorhombic [7] rather than tetragonal.

In this work, CuV_2S_4 grown by chemical vapour transport using $TeCl_4$ as the transporting agent has been studied. The temperature dependence of the magnetization has been measured at higher fields (1, 3, 5 T) than in previous works and the optical reflectance has been measured for the first time. In addition specific heat and resistivity measurements are used to characterize the crystals. As will be seen, the new magnetic and specific heat data are not in complete agreement with previous measurements and an attempt is made to correlate magnetic, transport and structural properties with the sample preparation technique.

2. Results

2.1. Magnetic measurements

The samples studied in this work were single crystals prepared by chemical vapour transport using $TeCl_4$ as the transporting agent [8]. Magnetization measurements made using a Quantum Design SQUID (superconducting quantum interference device) magnetometer are presented—as M/H ratios—in figure 1. The samples were field cooled at three different fields (1, 3 and 5 T) to 2 K and the magnetic moment measured as the samples were warmed to 350 K.

The overall shape and magnitude can be compared to previous measurements shown in the upper two left panels in figure 2. Note the discrepancy near 90 K: whereas the previous data show a sharp drop or at least a change in slope, the present data do not. It must be noted that

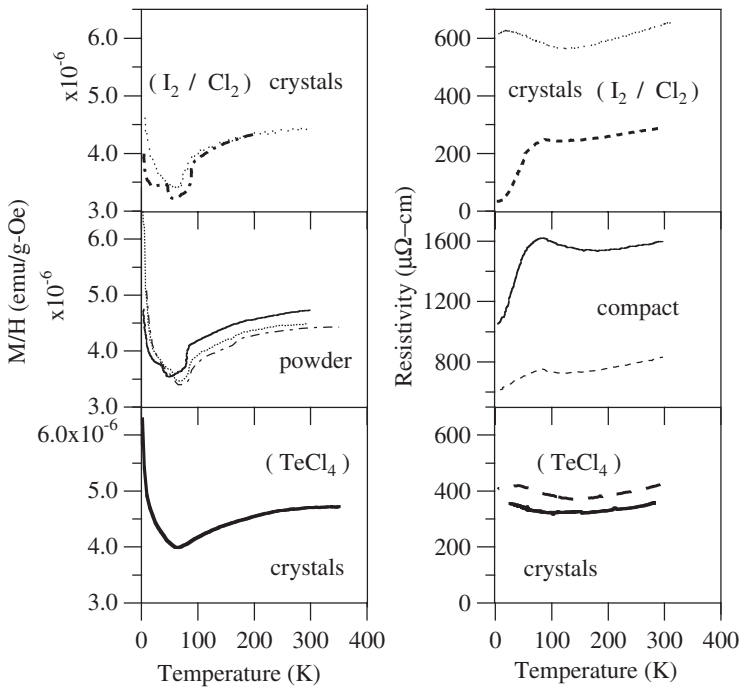

Figure 2. A comparison of previous measurements of magnetic susceptibility and resistivity of CuV_2S_4 samples prepared using various techniques. Upper two panels (crystals grown using chemical vapour transport using iodine (I_2) or chlorine (Cl_2) as the transporting agent) susceptibility (thick dot–dash line—[3], dots—[9]), resistivity (thick dashed line—[10], dots—[9]). Middle two panels (powders or compacts grown using standard evacuated silica containers) susceptibility (solid line—[5], dotted line—[11], thin dot–dashed line—[12]), resistivity (solid line—[5], long dash—[6]). Lower two panels (crystals grown using chemical vapour transport using $TeCl_4$ as the transporting agent) susceptibility (thick line: this work), resistivity (thick line—this work, thick long-dashed line—[8]).

while the magnitude of the slope change varies from sample to sample, complete suppression of the cusp is seen only in crystals grown using $TeCl_4$ as the transporting agent. Note also in figure 2 that whereas there is an anomaly in the resistivity at 90 K for polycrystalline samples, the anomaly is extremely suppressed for crystals grown using $TeCl_4$.

Two explanations have been offered for the susceptibility cusp: it has been associated with a cubic to tetragonal structural transition [11] or with CDW formation [12]. Specific heat measurements were made to explore whether the structural transition occurs in these crystals.

2.2. Specific heat

Since a peak in the specific heat had been previously observed at 91.9 K [10], specific heat measurements are a good indicator of the presence of the structural phase transition. Figure 3 presents the heat capacity of the same CuV_2S_4 crystal as is studied in figure 1. The most obvious difference from previous work [10] is the lack of a peak near 90 K. It is clear that the cubic–tetragonal transition does not occur in these crystals grown using $TeCl_4$ as the transporting agent. Other differences include the lack of structure near 55 K which had been associated with one of the CDW transitions [10].

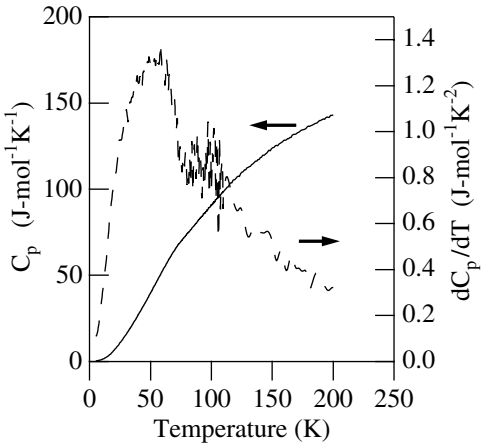

Figure 3. The heat capacity (solid line) versus temperature for CuV_2S_4. The derivative of the heat capacity (dashed line) is also shown.

2.3. Low temperature magnetic susceptibility

The magnetic data shown in figures 1 and 2 exhibit an increase in susceptibility below 50 K. Note that the high field data shown in figure 1 show a feature of the low temperature tail that is not seen in previous measurements [11]: observe that the magnetization is not proportional to the field at low temperatures—the M/H curves diverge—in the inset to figure 1. Some workers attribute the low temperature increase in susceptibility to paramagnetic impurities [3, 9] even though the low temperature tail is ubiquitous (see figure 2). The observation of Le Nagard *et al* that the tail is stronger for crystals grown by chemical vapour transport than for polycrystalline material highlights the importance of sample preparation [9]. The low temperature magnetic data can be explained using two mutually exclusive models: (i) non-interacting paramagnetic impurities; (ii) interacting magnetic moments.

The non-interacting paramagnetic impurity hypothesis can be explored by fitting the experimental magnetization data at low temperature (2–55 K) to the following equations [13]:

$$\begin{aligned} M &= \chi_0 H + N g J \mu_B B_J(x) \\ x &= g J \mu_B B / k_B T \\ B_J(x) &= \frac{2J+1}{2J}\operatorname{cotanh}\left(\frac{(2J+1)x}{2J}\right) - \frac{1}{2J}\operatorname{cotanh}\left(\frac{x}{2J}\right). \end{aligned} \tag{1}$$

The fit allows one to separate temperature independent contributions ($\chi_0 H$) to the low temperature magnetization—such as Pauli and Van Vleck paramagnetism, and core and Landau diamagnetism—from the contribution of impurity spins. It is also possible to determine some of the characteristics of the impurities (density (N), spin parameters g and J). The result of the fit to the experimental data is shown in figure 4 where it may be important to note that the temperature was varied while the field was fixed at 5 T.

Least squares fits determine the density of impurities N to be $0.050 \pm 0.005\%$ for all CuV_2S_4 molecules while χ_0, the constant contribution, is near $3.73 \pm 0.02 \times 10^{-6}$ emu g^{-1} Oe^{-1}. Energy dispersive x-ray measurements performed on these crystals indicate the presence of no substitutional impurities to the 0.1 at.% level. However, the impurity density suggested by the fits is below the sensitivity of the EDX measurements. It is also possible that any impurities are spins trapped on lattice imperfections, perhaps vacancies.

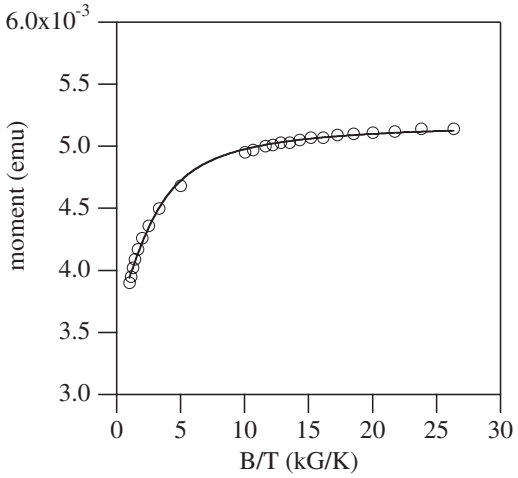

Figure 4. Magnetic moment versus ratio of field (B) to temperature (T) for the 5 T data set shown in figure 1. The experimental data are indicated by the circular markers. The solid line is a fit to equation (1). The sample was a single crystal of mass 0.0194 g.

While g and J are not totally independent in the fitting procedure, the product gJ is always $\approx 8.5 \pm 1$ regardless of what physically reasonable value of g is fixed for the fitting procedure. Thus the model suggests that there is an extremely large moment on these alleged impurities of about 9 bohr magnetons per centre. The possibly unrealistic value for the moment of the magnetic impurities may be an artefact of the assumption that the moments are non-interacting. On the other hand, extremely large moments have been seen in alloys of $Pd_{1-x}Fe_x$ where the iron atoms show extremely large moments (10 μ_B/Fe atom) due to spin polarization of the Pd d band [14]. There is some theoretical evidence for the tendency of the states at the Fermi level in CuV_2S_4 to spin polarize since they are of primarily V 3d character while the density of states is larger than in metallic V but slightly smaller than in metallic Pd [15, 16]. Recent calculations [17] have suggested that CuV_2S_4 in the cubic spinel structure should be a half-metallic ferromagnet.

A second possible model for the rise in susceptibility at low temperature allows for correlations between the moments. The magnetic moment measurements were fitted to a simple model consisting of, as before, a temperature independent contribution (χ_0) as well as a Curie–Weiss contribution. That is,

$$\chi = \chi_0 + \frac{C}{T + \theta}. \tag{2}$$

The fitting parameters are listed in table 1 while one can compare the experimental data to the models in figure 5. Note that the inset to the figure compares a Curie–Weiss fit, a simple Curie fit ($\theta = 0$ K) and the 1 T data set. Visual inspection suggests that the Curie–Weiss model fit is better. The positive values of θ for all the measurements suggest that there may be antiferromagnetic correlations between any localized moments existing in the samples. The same model was applied to previous workers' data (see figure 2) where the fitting parameters are listed in table 1. Note that, within experimental uncertainty, a positive θ value was obtained for all the measurements. Antiferromagnetic correlations are hard to understand given the small density of moments (<0.5% of all the molecules). It is also troubling, as table 1 indicates, that the fitting parameters are field dependent. This is very difficult to understand within a naive interpretation of equation (2). A similar field dependence

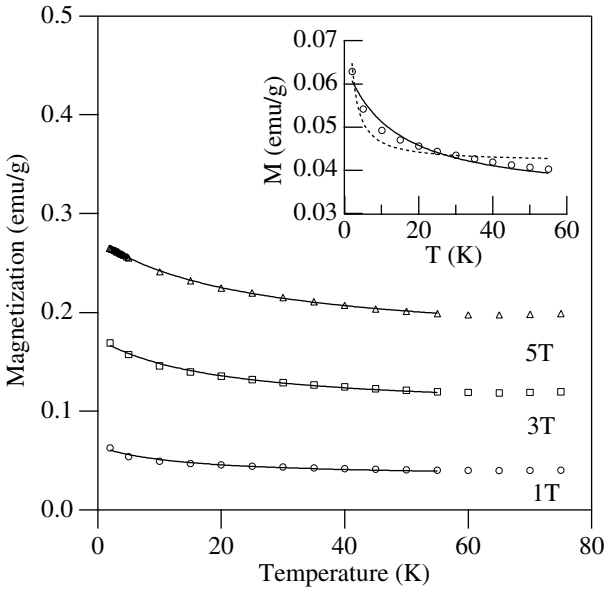

Figure 5. Magnetization versus temperature for three different applied fields (1, 3, 5 T). The samples were field cooled to 2 K, and the magnetic moment measured as the temperature was increased. The markers indicate experimental data, while the solid lines are fits to a model that consists of a temperature independent contribution and a Curie–Weiss contribution ($M/H = \chi_0 + \frac{C}{T+\theta}$). The fitting parameters are given in table 1. Inset: experimental magnetization versus temperature data (markers) taken at 1 T and two models. The solid line shows a model that consists of a temperature independent contribution and a Curie–Weiss contribution, while the dotted line shows a model that consists of a temperature independent contribution and a straight Curie contribution ($M/H = \chi_0 + \frac{C}{T}$).

Table 1. Magnetic susceptibility fitting parameters for the model discussed in the text. The χ_0, C and θ entries are in units of 10^{-6} emu g^{-1}, 10^{-6} emu K g^{-1} and K, respectively. There are also table entries for fits of the same model to the literature data shown in figure 2.

References	Temperature range (K)	χ_0	C	θ
This work (1 T)	(2–25)	4.09 ± 0.04	10 ± 1	2.7 ± 0.4
This work (3 T)	(2–25)	3.64 ± 0.16	27 ± 7	12 ± 3
This work (5 T)	(2–25)	3.24 ± 0.03	51 ± 2	24 ± 1
[3]	(4.3–21)	3.2 ± 0.4	2.8 ± 0.6	0.0 ± 0.8
[5]	(4.2–26)	3.4 ± 0.2	3.46 ± 0.04	4.6 ± 0.8
[11]	(2–26)	2.8 ± 0.3	33 ± 8	5.6 ± 1.7
[9]	(7–33)	3.2 ± 0.2	18 ± 6	5.6 ± 3.3

of parameters was observed—although not presented in this paper—in fits of the experimental data to equation (1). In the end, the low temperature susceptibility tail—which has also been observed for many ternary sulfospinels beside CuV_2S_4 [1, 2]—cannot be explained by a simple collection of independent moments and remains a puzzle. However, it is interesting to note that the minimum in magnetic susceptibility occurs at the same temperature (75 K) as the change in slope observed in the specific heat measurements of figure 3 suggesting a correlation between the 75 K CDW transition [3] and the magnetization.

Table 2. Fitting parameters for the model dielectric function (equation (3)) used to fit the reflectance data. The units of all parameters are cm^{-1} except for ϵ_∞ which is unitless.

ϵ_∞	ω_p	Γ
1.277 ± 0.004	$20\,200 \pm 30$	2740 ± 10
ω_{oL}	Γ_L	ω_{pL}
$16\,600 \pm 200$	$52\,000 \pm 2000$	$54\,000 \pm 1000$

2.4. Reflectance measurements

The samples were polished into plates parallel to one of the (111) crystal faces for reflectance measurements. The reflectance was measured at several temperatures between 40 and 300 K using a reflectometer similar to the one described in [18]. The key feature of the reflectometer is the use of *in situ* evaporation. The absolute reflectance is measured in two steps. The power spectrum of light reflected off of the sample is first measured at several temperatures. Then a gold film is evaporated onto the sample. Finally the power spectrum of the gold covered sample is measured at the same temperatures as before evaporation. The ratio of these two measurements, corrected for the reflectance of gold, is a measure of the absolute reflectance of the sample.

The inset to figure 6 shows the reflectance spectrum measured at 295 K between 70 and 20 000 cm^{-1}. Note the structure near 16 000 cm^{-1} which indicates the existence of a high frequency absorption process in addition to the current carriers responsible for the high reflectance at very low frequencies. The main part of figure 6 indicates that the reflectance spectrum between 70 and 2000 cm^{-1} at 40 and 295 K is approximately the same (to within the experimental uncertainty of ~1%). The optical data are consistent with the relative temperature independence of the dc resistivity of these particular crystals [8]. It is possible to model the reflectance using a dielectric function consisting of a Drude component (for the free carrier response) and a Lorentz oscillator (for the high frequency excitation):

$$\epsilon(\omega) = \epsilon_\infty - \frac{\omega_p^2}{\omega^2 + i\Gamma\omega} + \frac{\omega_{pL}^2}{(\omega_{oL}^2 - \omega^2) - i\Gamma_L\omega}. \tag{3}$$

The fitting parameters are listed in table 2 while the fits can be compared with the data in figure 6.

Figure 7 shows the real part of the optical conductivity at 295 K obtained via Kramers–Krönig transformation of the reflectance data using a Hagens–Rubens low frequency extrapolation consistent with the measured dc resistivity (360 $\mu\Omega$ cm) and a high frequency extrapolation created by the fits to the reflectance data discussed above. Note again that there appear to be two components in the spectrum: a low frequency component that one associates with the current carriers and a very broad absorption peak near 15 000 cm^{-1} (figure 7). Comparing the optical conductivity spectrum with the electronic band structure calculated by Lu *et al* [15], one might associate the high frequency component with excitations between S(3p) states just below and V(3d) states just above the Fermi level.

The plasma frequency obtained from the fits (see table 2 is approximately 20 000 cm^{-1}). If the bare electron mass is assumed, the carrier density obtained from the optical data is about 5×10^{21} cm^{-3} which is almost one carrier per formula unit and which is consistent with Hall measurements (p-type) assuming a single band model [5]. The mean free path at 300 K extracted from this carrier density and the Drude scattering rate (2700 cm^{-1}) is 11.5 Å, which is comparable to the spinel unit cell length of 9.8 Å.

There are several points that can be made concerning the optical data. The first is that there is little structure in the 70–1000 cm^{-1} region of the real optical conductivity spectrum of

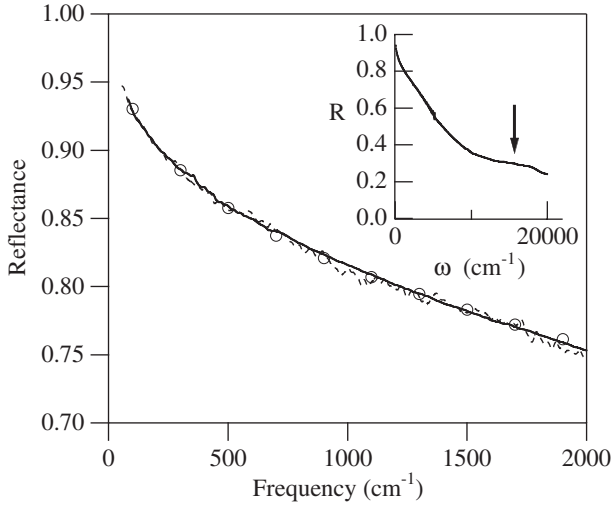

Figure 6. Reflectance spectrum of CuV_2S_4 at 295 K (solid line) and 40 K (dashed line). The data are compared to the model reflectance (open circles) generated from a dielectric function consisting of a Drude component and one Lorentz oscillator (see the text and table 2). Inset: room temperature reflectance (R) versus frequency (ω) for CuV_2S_4. The arrow indicates the position of a second absorption mechanism, besides that of the free carriers.

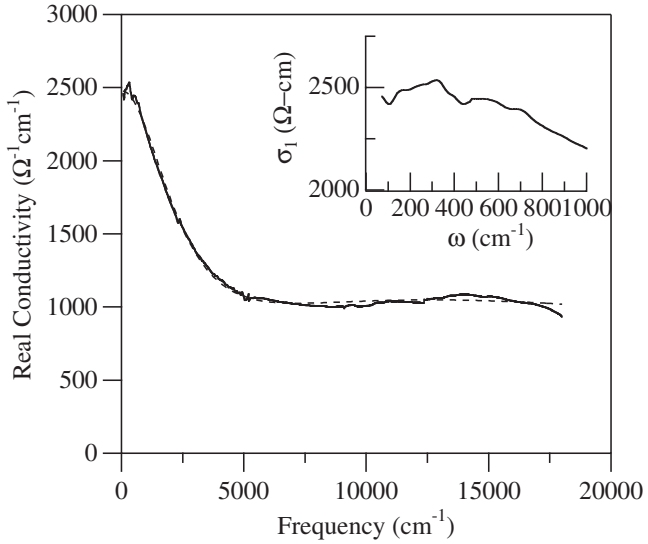

Figure 7. Real optical conductivity of CuV_2S_4 at room temperature (solid line) obtained by Kramers–Krönig analysis of the reflectance data. The data are compared to the optical conductivity generated from the dielectric function discussed in table 2. Inset: the low frequency real optical conductivity (σ_1) versus frequency (ω).

figure 7 in contrast to the case for the spectra of many metallic oxides [19] and silicides [20] with comparable resistivities (≈400 $\mu\Omega$ cm). The lack of prominent phonon peaks in the 70–1000 cm^{-1} region may be related to the low Debye temperature ($\theta_D = 205$ K) extracted from specific heat measurements [8]. In this interpretation the optical phonons have low frequencies

due to the large spaces in the sulfur sublattice for cations to vibrate. A second interpretation is that chemical bonds in CuV_2S_4 have little ionic character which is not in agreement with the calculated charge density [15] nor is it likely when simple binary transition metal sulfides exhibit strong restrahlen bands. It is more likely that the optical phonons are simply screened in CuV_2S_4 by the free carriers. Then, the phenomena that make optical phonons appear despite the presence of free carriers in the copper oxides (dynamic charge density inhomogeneity [19]) and silicides (coupling to an electronic continuum [20]) do not arise in CuV_2S_4.

Another point that can be made from the optical data is that there is no compelling evidence in figure 7 for the 100 cm^{-1} gap postulated by Yoshikawa *et al* [11] to explain the temperature dependence of the magnetic susceptibility between 100 and 300 K. The optical conductivity can be fitted by a simple two-component Drude–Lorentz model which requires only a free carrier and a high energy ($\approx$2 eV) interband response.

The relative temperature independence of the resistivity [8], the large scattering rate parameter of the Drude reflectance fit and the small mean free path all suggest a high degree of disorder. The optical conductivity appears to increase between 100 and 300 cm^{-1} in the inset to figure 7. It is possible that the slight depression of the low frequency conductivity is associated with weak localization of the carriers [21, 22]; however fitting with a weakly localized optical conductivity does not improve the χ^2 value significantly.

3. Discussion

It is interesting to try to correlate structural, magnetic and transport properties with the sample preparation technique. A reading of the literature reveals that all of the reports of the cubic–tetragonal structural transition (in particular splitting of the (400) line [6] in x-ray powder diffraction spectra) have been based on measurements on polycrystalline samples prepared in evacuated ampoules [5, 6, 12]. Significantly, Le Nagard *et al* grew crystals using chemical vapour transport using chlorine or iodine and observed no broadening or splitting of the (400) line in x-ray spectra well below 90 K [9]. This discrepancy may be due either to improved instrumental resolution in the Miyatani *et al* data [6] or to inhibition of the structural transition due to small differences in sample stoichiometry resulting from different methods of sample preparation.

Consider now the different measurements of electrical resistivity shown in the three right panels of figure 2. Note the two strikingly different low temperature behaviours: the resistivity either decreases dramatically or stays relatively constant below 90 K. All those groups that report a cubic–tetragonal transition observe a decrease in resistivity at low temperature. On the other hand, one group that measures cubic low temperature symmetry [9] also measures a relatively constant resistivity below 90 K (see the top right-hand panel in figure 2). Hence it is tempting to associate the resistivity decrease with a cubic–tetragonal structural transition and disorder as the factor that inhibits the cubic–tetragonal transition. A recent paper on high quality polycrystalline material confirms that samples exhibiting the cubic–tetragonal transition at 90 K also exhibit a cusp in magnetic susceptibility at the transition temperature and small residual resistivity ratios [23]. The optical measurements on crystals grown with $TeCl_4$ as the transporting agent which were discussed above suggested a small mean free path and perhaps weak localization and disorder probably related to the relatively constant resistivity at low temperature. The suppression of the 90 K structural transition may be related to this disorder.

It is interesting to consider the role that spin fluctuations might play in the other physical properties of CuV_2S_4. Lu *et al* found that electron–phonon coupling can account for less than half of the discrepancy between the experimental electronic specific heat and that predicted

from band structure [15]. Note that $\gamma \approx 50$ mJ K^{-2} for CuV_2S_4, which is almost as large as for some nearly ferromagnetic systems (e.g. Pd) where spin fluctuations are important. A second possible indication of the importance of spin fluctuations in CuV_2S_4 is in the resistivity data shown in figure 2. One might speculate that the sample with the lowest resistivity at 4 K is exhibiting the intrinsic behaviour of CuV_2S_4. These are the Sekine *et al* measurements on crystals grown using iodine as the transporting agent seen in the top right panel of figure 2.

Note that the lowest resistivity curve exhibits high temperature resistivity saturation and a T^2 dependence at low temperatures. Both of these features are similar to those for systems where spin fluctuations are important such as the Laves phase rare earth dicobalts [24] and the elemental actinides [25]. In spin fluctuation systems, the temperature at which the resistivity begins to saturate is a measure of the spin fluctuation energy and would be roughly 80 K for CuV_2S_4 according to figure 2. It is interesting to compare CuV_2S_4 with YCo_2. A least squares fit of the Sekine *et al* low temperature data for CuV_2S_4, shown in figure 2, to $\rho = \rho_0 + AT^2$ yields $A = 58$ nΩ cm K^{-2}. In comparison, $A = 16$ nΩ cm K^{-2} for YCo_2 and the resistivity begins to saturate at 200 K [24]. These values are crudely consistent with the prediction [25] that $A \propto 1/T_{sf}^2$.

4. Conclusions

It has been observed that the magnetization of CuV_2S_4 crystals grown using chemical vapour transport and $TeCl_4$ as the transporting agent do not exhibit the cusp in magnetic susceptibility near 90 K that is exhibited by powders or crystals grown using different transporting agents. Specific heat measurements made on the same crystal show no feature at 90 K associated with the structural transition. It is clear that the sharp drop in magnetization is associated with the structural transition and that this transition does not occur in CuV_2S_4 crystals grown using chemical vapour transport with $TeCl_4$ as the transporting agent. It has been observed that the magnetization of such crystals is not a linear function of the applied field below 20 K in CuV_2S_4. Analysis of the magnetization below 50 K has indicated that any magnetic impurities exhibit a large moment. Reflectance measurements on CuV_2S_4 crystals grown using chemical vapour transport and $TeCl_4$ as the transporting agent are consistent with those for a disordered metal. A high frequency absorption has been observed near 16 000 cm^{-1} in the real optical conductivity spectrum in addition to the free carrier absorption. It has been suggested that spin fluctuations may play an important role in the physical properties of CuV_2S_4.

Acknowledgments

The authors would like to acknowledge discussions with Dr S Bose as well as the financial support of NSERC.

References

[1] Hagino T, Seki Y, Wada N, Tsuji S, Shirane T, Kumagai K and Nagata S 1995 *Phys. Rev.* B **51** 12673
[2] Nagata S, Matsumoto N, Kato Y, Furubayashi T, Matsumoto T, Sanchez J P and Vuillet P 1998 *Phys. Rev.* B **58** 6844
[3] Fleming R M, DiSalvo F J, Cava R J and Waszcak J V 1981 *Phys. Rev.* B **24** 2850
[4] Matsuno J, Fujimori A, Mattheis L F, Endoh R and Nagata S 2001 *Phys. Rev.* B **64** 115116
[5] Van Bruggen C F 1982 *Ann. Chim. Fr.* **7** 171
[6] Tanaka T and Miyatani K 1997 *J. Phys. Soc. Japan* **66** 3341
[7] Mahy J, Colaitis D, Van Dyck D and Amelinckx S 1987 *J. Solid State Chem.* **68** 320

[8] Hagino T, Seki Y, Takayanagi S, Wada N and Nagata S 1994 *Phys. Rev.* B **49** 6822
[9] Le Nagard N, Katty A, Collin G, Gorochov O and Willig A 1979 *J. Solid State Chem.* **27** 267
[10] Sekine T, Uchinokura K and Iimura H 1984 *Solid State Commun.* **51** 187
[11] Yoshikawa Y, Wada S, Miyatani K, Tanaka T and Miyamoto M 1997 *Phys. Rev.* B **55** 74
[12] Kishimoto Y, Ohno T, Kanshiro T, Michichiro Y, Mizuno K, Miyamoto M, Tanaka T and Miyatani K 1995 *Solid State Commun.* **96** 23
[13] Kittel C 1976 *Introduction to Solid State Physics* 5th edn (New York: Wiley)
[14] DiSalvo F J and Wasczak J V 1982 *Phys. Rev.* B **26** 2501
[15] Lu Z W, Klein B M, Kurmaev E Z, Cherkashenko V M, Galakhov V R, Shamin S N, Yarmoshenko Yu M, Trofimova V A, Uhlenbrock S, Neumann M, Furubayashi T, Hagino T and Nagata S 1996 *Phys. Rev.* B **53** 9626
[16] Janak J F 1977 *Phys. Rev.* B **16** 255
[17] Park M S, Kwon S K and Min B I 2001 *Phys. Rev.* B **64** 100403
[18] Homes C C, Reedyk M, Crandles D A and Timusk T 1993 *Appl. Opt.* **32** 2976
[19] Homes C C, McConnell A W, Clayman B P, Bonn D A, Liang R, Hardy W N, Inoue M, Negishi H, Fournier P and Greene R L 2000 *Phys. Rev. Lett.* **84** 5391
[20] van der Marel D, Damascelli A, Schulte K and Menovsky A A 1998 *Physica* B **244** 138
[21] Basov D N, Puchkov A V, Hughes R A, Strach T, Preston J, Timusk T, Bonn D A, Liang R and Hardy W N 1994 *Phys. Rev.* B **49** 1216
[22] Lee K, Heeger A and Cao Y 1993 *Phys. Rev.* B **48** 14884
[23] Okada H, Koyama K and Watanabe K 2004 *J. Phys. Soc. Japan* **73** 3227
[24] Gratz E 1997 *Physica* B **237/238** 470
[25] Coqblin B, Iglesias-Sicardi J R and Jullien R 1978 *Contemp. Phys.* **19** 327